Proceedings of the ASME 2016 Heat Transfer Summer Conference
HT2016
July 10-14, 2016, Washington, DC, USA

HT2016-7414

THERMAL INTERFACIAL RESISTANCE REDUCTION BETWEEN METAL AND DIELECTRIC MATERIALS BY INSERTING INTERMEDIATE METAL LAYER

Xiangyu Li, Wonjun Park, Yong P. Chen, Xiulin Ruan
Purdue University
West Lafayette, Indiana 47907

ABSTRACT

In this work, we have observed 60% reduction in total interfacial resistance by adding an intermediate metal layer nickel between gold and aluminum oxide. Two temperature model is applied to explain the change of interfacial resistance, including both lattice mismatch with diffuse mismatch model and electron-phonon coupling effect. Simulation result agrees reasonably well with experimental data. Even though interfacial resistance due to electron-phonon coupling effect for Au-aluminum oxide is much larger than that of Ni-aluminum oxide interface, lattice mismatch is still the dominant factor for interfacial resistance.

NOMENCLATURE

b Half width of metal line
C_{rt} Coefficient between resistance and temperature
D Thermal diffusivity
DOS Phonon density of state
f Bose-Einstein distribution function
G_{ep} Electron-phonon coupling factor
h Thermal interfacial conductance
k Thermal conductivity
k_e Electron thermal conductivity
k_p Phonon thermal conductivity
l Length of metal line
p Power assumption of metal line
q^{-1} penetration depth
R_{diff} Thermal resistance difference
R_{ei} Inelastic electron scattering thermal resistance
R_{ep} Electron-phonon coupling thermal resistance
R_{pp} Phonon mismatch thermal resistance
T_e Electron temperature
T_p Phonon temperature
$v_{1\omega}$ Voltage signal of ω frequency
$v_{3\omega}$ Voltage signal of 3ω frequency
α Transmission coefficient
ΔT Temperature oscillation amplitude
ΔT_R Temperature oscillation amplitude for reference sample
ΔT_{F+R} Temperature oscillation amplitude for thin film sample
δ Kronecker delta function
$\hbar$ Plank's constant
ω Frequency of current in 3ω measurement

INTRODUCTION

It has become crucial to measure and evaluate thermal interfacial resistance between metal and dielectric materials, especially when thin films are widely applied in integrated circuits. As the thickness of films shrinks to micro/nano-scale, the interfacial resistance between metal and dielectric materials ($\sim 10^{-8}\text{m}^2\text{K/W}$ [1–5]) is becoming comparable to the thermal resistance of thin films ($\sim$10nm) in various engineering applications [6–8]. In these scenarios, interfacial thermal resistance has become a challenge for thermal management of nano-scale electronic devices. Gold has been widely used for electrical conductance due to its high conductance and chemical stability. However, thermal interfacial resistance between gold and dielectric materials is still less than optimal.

The theoretical estimation of interfacial resistance between metal and dielectric materials is of great interest by various

 Copyright © 2016 by ASME

groups. There are many approaches to estimate interfacial resistance, such as acoustic mismatch model (AMM) [9, 10], and diffuse mismatch model (DMM) [10]. These two models can reach reasonable agreement with experiments at low temperatures below 40K depending on different interface conditions. Certain modifications [8] are proposed for high temperatures, by introducing and relying on parameters fitted with experimental data, though the use of such fitting parameters may make the agreement coincidental. Atomic level simulations such as molecular dynamics [11–15], Green's function method [16, 17] have also been used for interfacial resistance, with inputs of only lattice structures and interatomic potentials. However, due to their high computational cost [11], they are more suitable for low-dimensional system. The methods mentioned above can only account for thermal transfer through phonons, ignoring the contribution of other carriers. For metals, semimetals, or heavily doped semiconductors where electron is main carrier of heat transfer, its contribution to heat transfer cannot be neglected. Due to differences in main heat carriers, electrons and phonons at different sides of the interface between metal and dielectric materials may have a large difference in kinetic energy, when electron-phonon coupling effect could be significant [18, 19]. It is more reasonable to combine both electron-phonon coupling effect with phonon mismatch model than to apply either of them alone. It is widely accepted that the metal-dielectric interfacial resistance includes not only phonon-phonon scattering, but also electron-phonon coupling effect at the interface as well as electron inelastic scattering across the interface. A simple approach to implement electron-phonon coupling effect is two-temperature model [18, 20–24], assuming two different temperatures for phonons and electrons separately across the interface.

In this work, we have fabricated three layered structures on silicon substrate, consisting of Ni, Au, and aluminum oxide layers. Thermal interfacial resistance characterization is done by 3ω method. We observed around 60% reduction of total interfacial resistance by adding nickel layer between gold and aluminum oxide. Two temperature model is applied to explain the change of interfacial resistance, including both lattice mismatch with diffuse mismatch model and electron-phonon coupling effect. Simulation results agree well with experimental results. Even though interfacial resistance due to electron-phonon coupling effect for Au-aluminum oxide is much larger than that for Ni-aluminum oxide, lattice mismatch is still the dominant factor for interfacial resistance between nickel, gold and aluminum oxide.

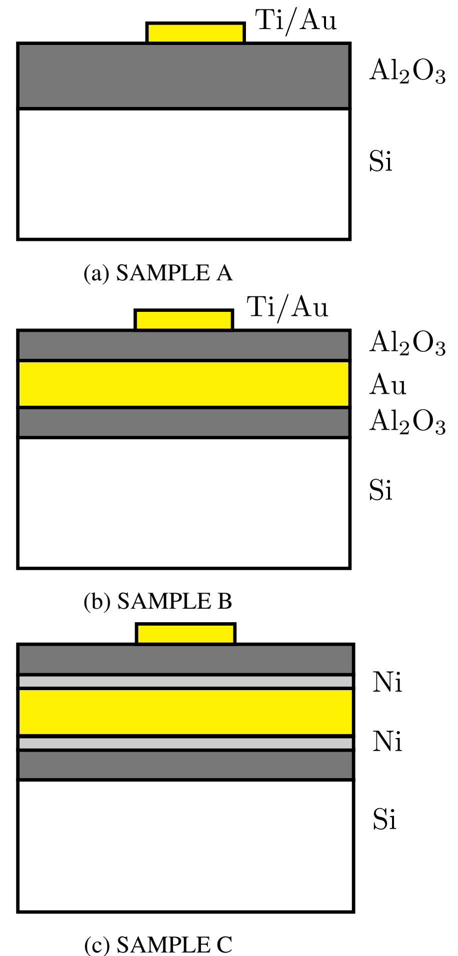

FIGURE 1: SANDWICH STRUCTURES FABRIACATED WITH MULTIPLE LAYERS

SAMPLE FABRICATION

Two sandwich structures and a reference sample are fabricated to determine interfacial resistance between gold and aluminum oxide layer, with and without nickel intermediate layer, shown in Fig.1, where white color stands for silicon substrate, yellow for gold layer, dark gray for aluminum oxide, and light gray for nickel. Silicon substrate is first cleaned with RCA method [25] (the Radio Corporation of America), and HF dip method to remove any oxidation layer and contamination. It is crucial to remove any oxidation layer due to low thermal conductivity of silicon oxide. The first structure, sample A, as the reference sample, has 60nm aluminum oxide layer on silicon substrate. The second one, sample B, consists of 30nm aluminum oxide layer, 50nm gold layer, and another 30nm aluminum oxide layer on top. And sample C inserts 20nm nickel layers between gold and aluminum oxide layers. Aluminum oxide layers are deposited with atomic layer deposition to ensure a consistent thickness, and metal layers are made with evaporation. Above the surfaces of all multi-layer structures, a metal line of 30μm wide and 3mm long is deposited with 20nm Ti and 100nm Au using photolithography for 3ω thermal characterization.

Copyright © 2016 by ASME

THERMAL INTERFACIAL RESISTANCE CHARACTERIZATION

The differential 3ω method [26] is used to characterize interfacial resistance in our work. It is developed to measure thin film thermal conductivity and interfacial resistance based on 3ω method [27, 28] that requires a thin metal line on the surface of the sample. Because of the micro-scale of the metal line, radiation loss even at high temperature is insignificant. During the measurement, an AC current of frequency ω is applied to the metal line, heating up the surface of the sample, resulting in a temperature oscillation amplitude of ΔT, and a voltage of 3ω frequency across the metal line. Three lock-in amplifiers are used to measure $v_{1\omega}$, $v_{3\omega}$ and power consumption p of the metal line. Detailed mathematic deductions can be found in previous literatures [27, 28]. For bulk materials, ΔT can be expressed as Eq.(1)

$$\Delta T = \frac{2v_{3\omega}}{v_{1\omega}C_{rt}} = \frac{p}{\pi k}\int_0^\infty \frac{sin^2(\lambda b)}{(\lambda b)^2(\lambda^2+2i\omega/D)^{1/2}}d\lambda \quad (1)$$

where k, D is the thermal conductivity and thermal diffusivity of the bulk sample, b is half width of metal line, and C_{rt} is temperature coefficient for metal line. For measurement of film conductivity or interfacial resistance, 2 structures are measured separately, one reference sample without thin films, another with thin films, leading to different ΔT of metal lines even with the same power consumption, according to Eq.(2). By subtracting temperature oscillation amplitude of reference sample from that of thin film structure, temperature drop across thin film can be obtained. If we define thermal impedance as temperature change over power consumption $\Delta T/p$, the thermal impedance difference between two samples can be calculated with Eq.(3).

$$\Delta T_{R+F} = \Delta T_R + \frac{p}{2bl}R_{diff} \quad (2)$$

$$R_{diff} = 2bl\left(\left(\frac{\Delta T}{p}\right)_{R+F} - \left(\frac{\Delta T}{p}\right)_R\right) \quad (3)$$

Results from 3ω measurement are shown in Fig.2. Comparing results of sample B and sample C with reference sample A, we can obtain thermal impedance difference ΔR_1, and ΔR_2 as in Eq.(7), (8), where interfacial resistance between Ni and Au is neglected due to its small value. We observed around 60% reduction of total interfacial resistance (from $9.52\times10^{-8}\mathrm{m^2K/W}$ to $2.68\times10^{-8}\mathrm{m^2K/W}$) by adding nickel layer between gold and aluminum oxide. With differential 3ω method, thermal interfacial resistance between gold and aluminum oxide is $4.84\pm0.13\times10^{-8}\mathrm{m^2K/W}$, and that between nickel and aluminum oxide is $1.40\pm0.14\times10^{-8}\mathrm{m^2K/W}$.

$$R_A = 2R_{AlO} + R_{Si-AlO} \quad (4)$$

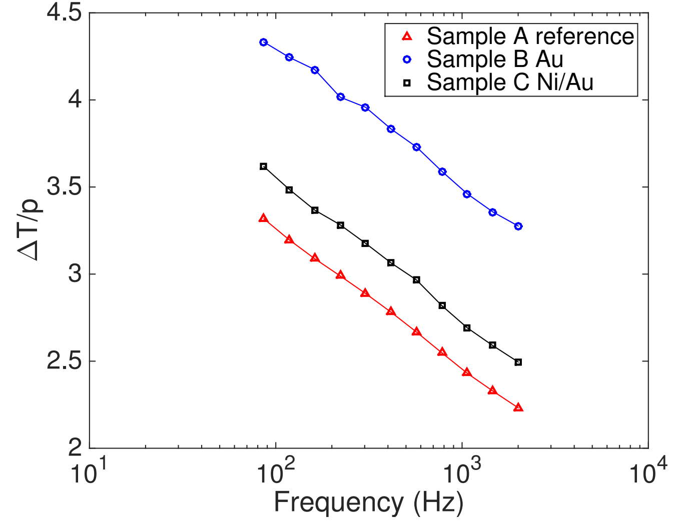

FIGURE 2: 3ω MEASUREMENT FOR THREE SANDWICH STRUCTURES

$$R_B = 2R_{AlO} + R_{Si-AlO} + 2R_{Au-AlO} \quad (5)$$

$$R_C = 2R_{AlO} + R_{Si-AlO} + 2R_{Ni-AlO} + R_{Au-Ni} \quad (6)$$

$$\Delta R_1 = R_B - R_C = 2R_{Au-AlO} \quad (7)$$

$$\Delta R_2 = 2R_{Ni-AlO} + R_{Au-Ni} \approx 2R_{Ni-AlO} \quad (8)$$

TWO TEMPERATURE MODEL ON INTERFACES

Two-temperature model assumes two different temperatures for phonons and electrons separately across the interface. The overall interfacial resistance consists of a phonon-phonon component R_{pp}, an electron-phonon component R_{ep}, as well as electrical inelastic scattering one, as shown in Fig.3 [29]. The third one R_{ei} is usually neglected due to its much higher resistance, since electron density in dielectric materials is low.

The first effect is the same with that for interfaces between dielectric-dielectric materials, where phonons in one side of interface transfer into the other side. Detailed diffuse mismatch model is applied to model phonon-phonon interface resistance in this work [10], which assumes phonons lose their correlations and randomize directions across the interface. Detailed phonon dispersions are calculated by lattice dynamics for nickel, gold and aluminum oxide in Fig.4. It should be noted that nickel is polycrystalline and aluminum oxide is amorphous in experiments due to the limitations of fabrication, while in lattice dynamics we assume crystalline structure for simplifications. In Fig.4, there are numerous branches of phonons for aluminum oxide. However, phonon frequencies in nickel and gold only overlap mostly with the acoustic phonons in aluminum oxide.

Copyright © 2016 by ASME

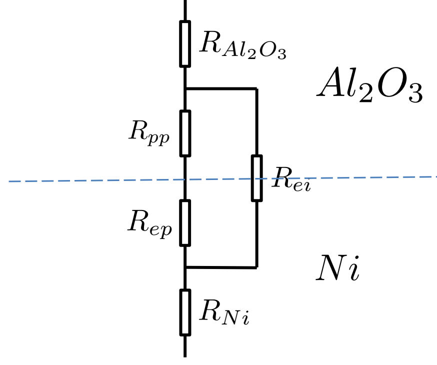

FIGURE 3: Thermal Resistance Network Between Nickel and Aluminum Oxide

So only these acoustic branches of aluminum oxide phonons are considered in the DMM calculation, since transmission between metal phonons and the other phonons of aluminum oxide is negligible. Detailed balance is enforced as $\alpha_{A\to B} = \alpha_{B\to A}$ to obtain transmission coefficient α. Equation(9), (10) are used for calculating interfacial resistance from material A to material B,

$$h_{A\to B} = \frac{1}{4}\sum_j \int \hbar\omega DOS_{A,j} v_{A,j} \alpha_{A\to B} \frac{\partial f}{\partial T} d\omega \tag{9}$$

$$\alpha_{A\to B}(\omega') = \frac{\sum_j DOS_{B,j}(\omega) v_{B,j}(\omega)\delta_{\omega',\omega}}{\sum_j DOS_{A,j}(\omega) v_{A,j}(\omega)\delta_{\omega',\omega} + \sum_j DOS_{B,j}(\omega) v_{B,j}(\omega)\delta_{\omega',\omega}} \tag{10}$$

where h is thermal interface conductance, $\hbar$ is Planck's constant, $DOS_{A,j}$ is the phonon density of state for mode j, material A, v is the group velocity, f is the Bose-Einstein distribution function, α is the transmission coefficient, δ is Kronecker delta function. Regarding to electron-phonon coupling effect, two different temperatures assigned for electrons and phonons are coupled as Eq.(11),(12),

$$k_e \frac{\partial^2 T_e}{\partial z^2} - G_{ep}(T_e - T_p) = 0 \tag{11}$$

$$k_p \frac{\partial^2 T_p}{\partial z^2} + G_{ep}(T_e - T_p) = 0 \tag{12}$$

where G_{ep} is the electron-phonon coupling factor for metal materials [21, 30], k_e is the electron thermal conductivity and k_p is the lattice thermal conductivity of the metal, calculated with non-equilibrium molecular dynamics (NEMD). Since electrons are main carriers for heat transfer in most metals, $k_e \gg k_p$. With further mathematical deductions, interfacial resistance based on

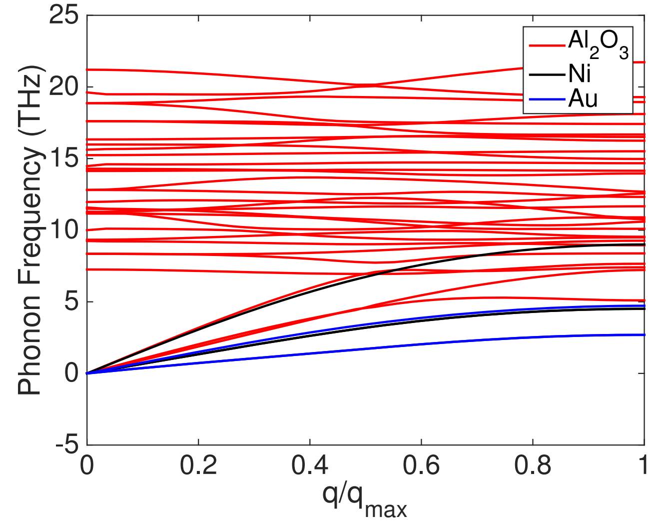

FIGURE 4: PHONON DISPERSION OF NI, AU, AND ALUMINUM OXIDE

two temperature model can be written as Eq.(13) [24],

$$\begin{aligned} R_i &= R_{pp} + R_{ep} = \frac{1}{h_{pp}} + (\frac{k_e}{k_e + k_p})^{3/2} (\frac{1}{G_{ep} k_p})^{1/2} \\ &\approx \frac{1}{h_{pp}} + (\frac{1}{G_{ep} k_p})^{1/2} \end{aligned} \tag{13}$$

where R_i is the overall thermal interfacial resistance, R_{pp}, h_{pp} are lattice mismatch resistance and conductance respectively, and R_{ep} is interfacial resistance regarding to electron-phonon coupling effect.

In our study, theoretical estimations using TTM are shown in Tab.1 along with experiment results. Even through nickel has a much larger electron-phonon coupling factor, thus smaller electron-phonon resistance than gold, lattice mismatch still dominates interfacial resistance for both Ni and Au. Compared with gold, phonons in nickel share larger frequency domain with those in aluminum oxide, thus phonon-phonon resistance is lower than Au.

CONCLUSION

In this work, we measured thermal interfacial resistance between nickel and aluminum oxide, as well as that between gold and aluminum oxide. A 60% decrease of total resistance is observed when an intermediate metal layer nickel is inserted between gold and aluminum oxide layers. Theoretical calculation of two temperature model shows similar results with experiments, which also indicates the dominance of phonon mismatch between these two metals and aluminum oxide.

Copyright © 2016 by ASME

TABLE 1: COMPARISON BETWEEN TTM AND 3ω MEASUREMENT

R_i^*	DMM	e-p coupling	TTM	Experiement
Ni-Al_2O_3	3.04	0.44	3.48	14.0
Au-Al_2O_3	5.16	2.64	7.80	48.4

* $10^{-9} m^2 K/W$

ACKNOWLEDGMENT

Thanks go to Tianli Feng and Yan Wang for their help in two temperature model and phonon dispersion.

REFERENCES

[1] Lee, S.-M., and Cahill, D. G., 1997. "Heat transport in thin dielectric films". *Journal of Applied Physics,* ***81***(6), mar, p. 2590.

[2] Stoner, R. J., and Maris, H. J., 1993. "Kapitza conductance and heat flow between solids at temperatures from 50 to 300 K". *Physical Review B,* ***48***(22), dec, pp. 16373–16387.

[3] Stevens, R. J., Smith, A. N., and Norris, P. M., 2005. "Measurement of Thermal Boundary Conductance of a Series of Metal-Dielectric Interfaces by the Transient Thermoreflectance Technique". *Journal of Heat Transfer,* ***127***(3), mar, p. 315.

[4] Griffin, A. J., Brotzen, F. R., and Loos, P. J., 1994. "Effect of thickness on the transverse thermal conductivity of thin dielectric films". *Journal of Applied Physics,* ***75***(8), apr, p. 3761.

[5] Kim, J. H., Feldman, A., and Novotny, D., 1999. "Application of the three omega thermal conductivity measurement method to a film on a substrate of finite thickness". *Journal of Applied Physics,* ***86***(7), oct, p. 3959.

[6] Cola, B. a., Xu, J., Cheng, C., Xu, X., Fisher, T. S., and Hu, H., 2007. "Photoacoustic characterization of carbon nanotube array thermal interfaces". *Journal of Applied Physics,* ***101***(5), pp. 1–9.

[7] Dames, C., 2004. "Theoretical phonon thermal conductivity of Si/Ge superlattice nanowires". *Journal of Applied Physics,* ***95***(2), p. 682.

[8] Prasher, R. S., and Phelan, P. E., 2001. "A Scattering-Mediated Acoustic Mismatch Model for the Prediction of Thermal Boundary Resistance". *Journal of Heat Transfer,* ***123***(1), p. 105.

[9] Little, W. A., 1959. "THE TRANSPORT OF HEAT BETWEEN DISSIMILAR SOLIDS AT LOW TEMPERATURES". *Canadian Journal of Physics,* ***37***(3), pp. 334–349.

[10] Swartz, E., and Pohl, R., 1989. "Thermal boundary resistance". *Reviews of Modern Physics,* ***61***(3), jul, pp. 605–668.

[11] Landry, E. S., and McGaughey, A. J. H., 2009. "Thermal boundary resistance predictions from molecular dynamics simulations and theoretical calculations". *Physical Review B,* ***80***(16), p. 165304.

[12] Diao, J., Srivastava, D., and Menon, M., 2008. "Molecular dynamics simulations of carbon nanotube/silicon interfacial thermal conductance.". *The Journal of chemical physics,* ***128***(16), p. 164708.

[13] Vallabhaneni, A. K., Qiu, B., Hu, J., Chen, Y. P., Roy, A. K., and Ruan, X., 2013. "Interfacial thermal conductance limit and thermal rectification across vertical carbon nanotube/graphene nanoribbon-silicon interfaces". *Journal of Applied Physics,* ***113***(6), p. 064311.

[14] Hu, L., Desai, T., and Keblinski, P., 2011. "Determination of interfacial thermal resistance at the nanoscale". *Physical Review B - Condensed Matter and Materials Physics,* ***83***(19), p. 195423.

[15] Hu, M., Keblinski, P., Wang, J.-S., and Raravikar, N., 2008. "Interfacial thermal conductance between silicon and a vertical carbon nanotube". *Journal of Applied Physics,* ***104***(8), p. 083503.

[16] Hopkins, P. E., Norris, P. M., Tsegaye, M. S., and Ghosh, A. W., 2009. "Extracting phonon thermal conductance across atomic junctions: Nonequilibrium Green's function approach compared to semiclassical methods". *Journal of Applied Physics,* ***106***(6), p. 063503.

[17] Huang, Z., Fisher, T. S., and Murthy, J. Y., 2010. "Simulation of thermal conductance across dimensionally mismatched graphene interfaces". *Journal of Applied Physics,* ***108***(11), p. 114310.

[18] Majumdar, A., and Reddy, P., 2004. "Role of electron-phonon coupling in thermal conductance of metalnonmetal interfaces". *Applied Physics Letters,* ***84***(23), p. 4768.

[19] Dechaumphai, E., Lu, D., Kan, J. J., Moon, J., Fullerton, E. E., Liu, Z., and Chen, R., 2014. "Ultralow thermal conductivity of multilayers with highly dissimilar Debye temperatures.". *Nano letters,* ***14***(5), may, pp. 2448–55.

[20] Duffy, D. M., and Rutherford, A. M., 2007. "Including the effects of electronic stopping and electronion interactions in radiation damage simulations". *Journal of Physics: Condensed Matter,* ***19***(1), p. 16207.

[21] Lin, Z., Zhigilei, L., and Celli, V., 2008. "Electron-phonon coupling and electron heat capacity of metals under conditions of strong electron-phonon nonequilibrium". *Physical Review B,* ***77***(7), feb, p. 075133.

[22] Koči, L., Bringa, E. M., Ivanov, D. S., Hawreliak, J., McNaney, J., Higginbotham, A., Zhigilei, L. V., Belonoshko, A. B., Remington, B. A., and Ahuja, R., 2006. "Simulation

Copyright © 2016 by ASME

of shock-induced melting of Ni using molecular dynamics coupled to a two-temperature model". *Physical Review B,* ***74***(1), p. 012101.

[23] Jones, R. E., Templeton, J. A., Wagner, G. J., Olmsted, D., and Modine, N. A., 2010. "Electron transport enhanced molecular dynamics for metals and semi-metals". *International Journal for Numerical Methods in Engineering,* ***83***(8-9), aug, pp. 940–967.

[24] Wang, Y., Ruan, X., and Roy, A. K., 2012. "Two-temperature nonequilibrium molecular dynamics simulation of thermal transport across metal-nonmetal interfaces". *Physical Review B,* ***85***(20), may, p. 205311.

[25] Kern, W., and Puotinen, D. a., 1970. "Cleaning solutions based on hydrogen peroxide for use in silicon semiconductor technology". *Rca Review,* ***31***(2), pp. 187–206.

[26] Borca-Tasciuc, T., Kumar, a. R., and Chen, G., 2001. "Data reduction in 3ω method for thin-film thermal conductivity determination". *Review of Scientific Instruments,* ***72***(4), p. 2139.

[27] Cahill, D. G., 1990. "Thermal conductivity measurement from 30 to 750 K: the 3ω method". *Review of Scientific Instruments,* ***61***(2), p. 802.

[28] Cahill, D. G., 1989. "Thermal conductivity of thin films: Measurements and understanding". *Journal of Vacuum Science & Technology A: Vacuum, Surfaces, and Films,* ***7***(3), may, p. 1259.

[29] Li, Z., Tan, S., Bozorg-Grayeli, E., Kodama, T., Asheghi, M., Delgado, G., Panzer, M., Pokrovsky, A., Wack, D., and Goodson, K. E., 2012. "Phonon dominated heat conduction normal to Mo/Si multilayers with period below 10 nm.". *Nano letters,* ***12***(6), jun, pp. 3121–6.

[30] Phillips, C. L., and Crozier, P. S., 2009. "An energy-conserving two-temperature model of radiation damage in single-component and binary Lennard-Jones crystals". *Journal of Chemical Physics,* ***131***(2009), pp. 0–11.

Copyright © 2016 by ASME